IEEE Access
Multidisciplinary | Rapid Review | Open Access Journal

Received December 21, 2018, accepted December 25, 2018, date of publication December 28, 2018,
date of current version January 23, 2019.

*Digital Object Identifier 10.1109/ACCESS.2018.2890024*

# Vibration Detection of Spanning Subsea Pipelines by Using a Spherical Detector

**GUO LIN, ZENG ZHOUMO, HUANG XINJING, LI JIAN, AND CHEN SHILI**

State Key Laboratory of Precision Measuring Technology and Instruments, Tianjin University, Tianjin 300072, China
Binhai International Advanced Structural Integrity Research Centre, Tianjin 300072, China

Corresponding author: Huang Xinjing (huangxinjing@tju.edu.cn)

This work was supported by the National Natural Science Foundation of China under Grant 51604192, Grant 61773283, and Grant 61473205.

**ABSTRACT** This paper proposes a method for detecting the vibration of subsea spanning pipelines by using a spherical detector (SD) equipped with a triaxial accelerometer. The mathematical analyses and experiments demonstrate that the acceleration modulus square (AMS) and the AMS of the ac components (AMS_AC) of the acceleration signals recorded by the SD have one characteristic component whose frequency is equal to and can be used to determine the pipeline vibration frequency. As the amplitude of this component is immune to the rotation noises of the SD, its signal-to-noise ratio is higher than that of other components whose frequencies are the mixture of the vibration and rotation frequencies. Removing the dc bias along the three sensitive axes can eliminate other characteristic frequencies to make the AMS_AC having the unique frequency to indicate the pipeline vibration. The vibration frequency can be accurately and sensitively identified by using the AMS_AC. The detection thresholds of 5-, 10-, and 15-Hz vibrations are 0.6, 0.4, and 0.2 mm with regard to the amplitude, respectively.

**INDEX TERMS** Subsea pipeline, spanning, vibration detection, acceleration, spherical detector.

## I. INTRODUCTION

Subsea pipelines are most important infrastructure for offshore oil and gas transportation, well known as ''the lifeline of the development and production of offshore oil and gas fields''. Security issues of subsea pipelines have always been drawing widespread attention. On one hand, once subsea pipelines fracture, the leaked oil will rapidly spread, leading to severe and widespread environmental pollution and even ecological disasters. On the other hand, it is extremely expensive and complicated to maintain and repair damaged subsea pipelines. There are many factors that can cause subsea pipeline to fatigue, [1]–[3] including chemical corrosion, scour erosion by the internal and external flows, and large external force or deformation, such as trawl and anchor dragging, spanning and vibration due to ocean current scouring, earthquake, and seabed displacement. Among those external force damages, the spanning vibration often occurs and occupies a large proportion.

In one hand, the spanning unavoidably occurs when the pipelines are laid on the seabed because of the unevenness of the seabed. On the other hand, long-term scour by the ocean current will wash away the sediment below the subsea pipeline to form new cavities below the pipelines, and then the subsea pipelines span [4], [5]. When the current flows across the spanning pipeline, it will generate alternating vortices and cause the spanning pipeline to vibrate [6], [7], which is called vortex-induced vibrations. The spanning length increase as the current induced erosion increases, and the resonance frequency of the spanning pipeline decreases. In general, the spanning length of subsea pipelines is 5m-60m, and the corresponding response frequency is between 0.5-20Hz, with 0.5-8Hz being more common [8], [9] When the frequency of the vortex release is close to the resonance frequency of the spanning pipeline, the pipeline will resonate, thereby entering the state of large vibrations. The corresponding vibration amplitude can be as high as 0.7m or higher. Spanning and severe vibration makes the subsea pipeline suffer from additional axial stresses and fatigue loads, which seriously threaten the pipeline safety and will eventually lead to fatigue damages [8]. If the vibration of the spanning pipeline is detected in time, remedial measures of landfill and reinforcement can be taken in advance to avoid pipeline collapses. Therefore, monitoring or quasi-real-time detection of subsea pipeline spanning is particularly significant.

The research on subsea pipeline spanning mainly focuses on the mechanical response analyses of the spanning sections

under waves and currents [6], [10], [11], and the stability and reliability assessment [12], [13] of subsea pipelines. These studies provide forward guidance for how to safely lay subsea pipelines to avoid spanning and how to predict the spanning existence, but do not address how to directly detect existing spanning for pipeline reinforcement [13]. People have also make many efforts on judging the possibility of pipeline spanning based on computational fluid dynamics, structural finite element analyses, and associated fluid-structure interaction [14]–[16]. The influences of pipeline specifications and support conditions are sophisticatedly modeled to judge whether spanning will occur and predict the resonance frequency of the free spanning subsea pipeline [14], [15]. By predicting current-induced scour beneath subsea pipelines in areas with small spanning depths, the reliability of the free spanning pipeline can be assessed in advance and large spanning can be avoided by backfilling dinas or installing extra supports [12], [16]. Since many of the model parameters are simplified, screening may be too strict or too loose, leading to excessive reinforcement or missed inspections. The reliability of spanning prediction is not as good and reliable as monitoring or quasi-real-timed detections.

For existing subsea pipeline spanning, one kind of detection methods are implemented via shape and appearance measurements from the outside or inside. Underwater robot with sonars or and underwater cameras, such as ROV (Remotely Operated Vehicle) [17] and AUV (Autonomous Underwater Vehicle) [18], [19], can be used for observing and looking for pipeline spanning via acoustic or optical imaging. However, the cost is extremely high. The difficulty and cost of deploying ROV and AUV will sharply increase with the increase of depth. Inner PIGs (Pipeline Inspection Gauges) [20], [21] with inertial navigation can also be used to identify very long spanning sections that have sunk and deformed via highly precise pipeline trajectory measurements to find the local abrupt change of the trajectory. However, because PIGs are bulky and in contact with the pipe wall tightly like a piston, they are susceptible to pipe deformation and bending. High risk of blockage limits their applications in subsea pipeline spanning inspections.

As vortex induced vibration is an important feature of a subsea spanning pipeline, a lot of efforts have been made on remotely sensing and reliably transmitting such vibration information for subsea pipeline spanning detections. Optical fiber is one of the most commonly used methods for monitoring pipeline vibrations [22]. Fiber optic sensing offers the ability to passively measure and transmit strain and vibration signals over tens of kilometers in a single fiber that lays along the pipeline. Commercially available fiber optic sensors are discrete Fiber Bragg Gratings (FBGs) [23]–[25] and fully distributed Optical Time Domain Reflectometry (OTDR) [25], [26]. Both FBGs and OTDR can remotely sense and monitor the vibration of the spanning pipeline, as the vibration induced optical signal can transmit over hundreds of kilometers. FBGs are usually used to monitor the sections where spanning may occur with high risk via being adhered to several points. The OTDR can distributedly sense and monitor the vibration of the entire pipeline by analyzing the Rayleigh, Brillouin or Raman backscattered spectra.

Accelerometers can also be used to measure the vibration of a spanning pipeline, but need to be fixed on the subsea pipeline and can only monitor one point per module [27]. In order to obtain the vibration signals of the pipeline in real time, underwater acoustic communication is required to establish a network consisting of many sensing nodes, relay nodes, and even underwater robots, etc [28], [29]. As all nodes are battery powered, their continuous working time is not long enough. Moreover, the cost of building an underwater communication network and the maintenance fee is too high. Another alternative method is to use a mobile detector carrying an accelerometer inside the pipeline to record the pipeline vibration, and the vibration is identified via off-line signal processing [30]. The in-pipe detector can detect the entire long pipeline without omissive sections and is not affected by the harsh external environment.

Spherical detector (SD) is a new promising method for pipeline inspections initially proposed and developed independently by Richard and Muthu [31] and Guo *et al.* [32], [33] for leakage detections. Recently, the latest promising uses of the SD and its advantages of quasi-real-time detection are demonstrated via subsea pipeline 3D localization [34], pipeline inclination measurement [35], inflection point detection, and magnetic anomaly detection [36]. Unlike the PIG, which has to run in tight contact with the pipe wall like a piston, the SD can freely roll forward inside the pipelines with no risk of blockage, as its diameter is smaller than the pipeline's. The SD can be used for densely launching and quasi-real-time subsea pipeline spanning monitoring thanks to its great convenience of employment compared to traditional PIGs: costing much less time for launch and retrieve, moving faster than the PIG, and with no risk of blockage [33].

The SD is a potential and promising method for quasi-real-time detections of pipeline spanning. However, as the SD is rolling while inspecting, any signal recorded is modulated by rotation and is therefore periodic and messy. It is very challenging to directly identify the vibration information of the spanning pipeline from the modulated inspection signals. This paper proposes a practicable method of detecting the vibration of subsea spanning pipelines by using the SD carrying an accelerometer. The average density of the SD is greater than that of oil, so the SD rolls forward at the bottom of the pipeline. Inside the vibration sections, the SD vibrates together with the pipeline. The acceleration signals measured will contain the information of the pipe vibration, the SD rotation, and the motion noise of the SD caused by the unsteady flow. This paper will demonstrate how to accurately identify the pipeline vibration by using the acceleration signals recorded by the SD through mathematical analyses and experimental tests. The performances of three methods, single acceleration component (SAC), acceleration modulus square (AMS), and the AMS of the AC components (AMS_AC) of

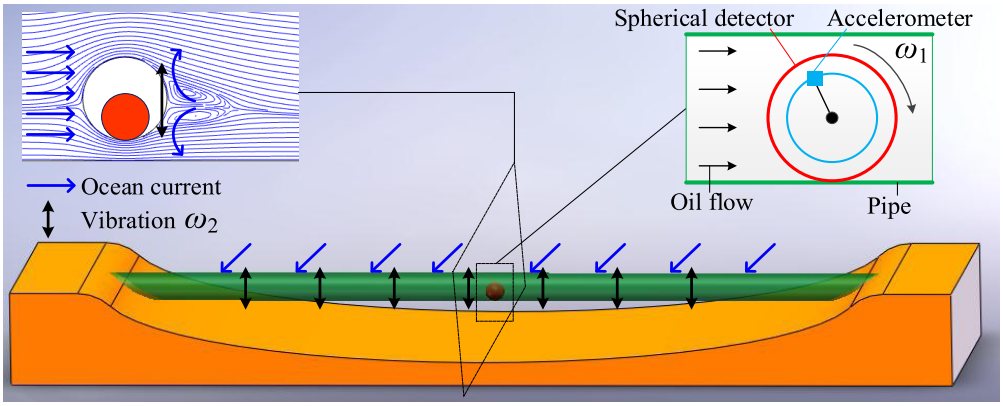


**FIGURE 1.** Schematic of vortex induced vibration detection of a spanning subsea pipeline.

the acceleration signals recorded by the SD, will be analyzed and compared both mathematically and experimentally.

## II. DETECTION PRINCIPLES

As shown in Figure 1, when the ocean current flows across a spanning pipeline on the seabed, swirls alternately appear up and down behind the pipeline, causing the pipeline to vibrate. The SD with an accelerometer and a data recorder inside is launched into the pipeline. Driven by the oil flow, the SD rolls forward and records the acceleration of the carrier. After the inspection is finished, the SD is retrieved from the pipeline and connected with the computer for the data to be downloaded. The vibration of the pipeline is identified by processing the acceleration signals offline. Previous studies have shown that the SD can always roll on the bottom of the pipeline without blockage and can smoothly pass through the vertical pipeline via reasonably designing the mass distribution, the average density, and the diameter ratio of the SD to the pipeline [33]. The SD can keep rotating around a fixed axis. Because the SD is always in contact with the pipeline wall, while rolling forward, it will vibrate together with the vibrating pipeline section. Therefore, the acceleration signals recorded by the SD contain not only the rolling information but also the pipe vibration information.

When the pipeline does not vibrate, any single acceleration component (SAC) of the accelerometer in the rolling SD is:

$$a_x = g\cos(\theta_0)\cos(\omega_1 t + \varphi_1) + A_1\cos(\theta_1) \tag{1}$$

Wherein, $\theta_0$ is the minimum angle between the accelerometer axis $x$ and the gravity acceleration; $\omega_1 = 2\pi f_1$, $f_1$ is the rolling frequency of the SD; $\theta_1$ is the angle between the centripetal acceleration and the accelerometer axis $x$. As the SD rolls forward, the accelerometer's trajectory is a circle in the vertical plane that is parallel to the pipe axis. Denote the radius of the circle as $r$, then the centripetal acceleration $A_1 = \omega_1^2 r$. The relationship of any one sensitive axis of the accelerometer, the gravity acceleration, and the centripetal acceleration is shown in Figure 2.

Since the ocean current is parallel to the seabed and the vortex-induced vibration is perpendicular to the ocean

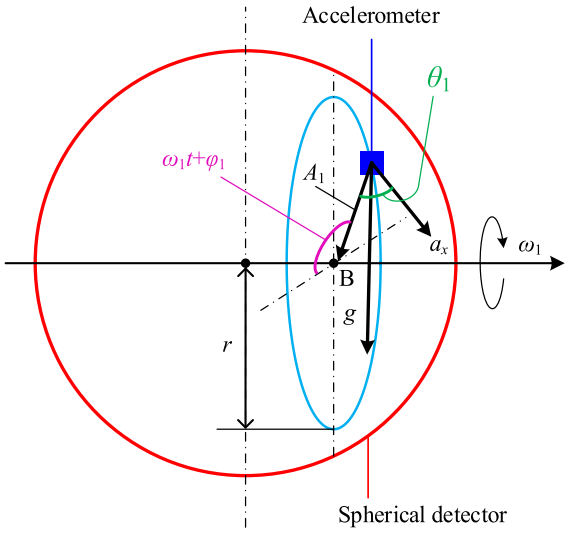


**FIGURE 2.** Posture of the accelerometer's sensitive axis inside a rotating SD.

current, the excitation exerted on the pipeline by the current is vertical. The SD vibrates up and down together with the pipeline. Because the density of the SD is larger than that of the oil inside the pipeline, the SD always keeps in touch with the bottom of the pipeline while rolling forward. Therefore, the SD has the same vibrational displacement at any moment as the pipeline. Denoting the vibration amplitude as $H_2$ and the vibration angular frequency as $\omega_2$, the displacement $dis(t)$ of the SD and the pipeline can be expressed as $dis(t) = H_2\cos(\omega_2 + \varphi_2)$, then the acceleration in the vertical direction caused by the vibration is $a(t) = dis(t)'' = H_2\omega_2^2\cos(\omega_2 + \varphi_2)$. The new total equivalent gravitational acceleration is $g + A_2\cos(\omega_2 + \varphi_2)$, where $A_2 = \omega_2^2 H_2$. Therefore, when the pipeline vibrates, any SAC of the accelerometer in the SD is:

$$a_x = [g + A_2\cos(\omega_2 t + \varphi_2)]\cos(\theta_0)\cos(\omega_1 t + \varphi_1) + A_1\cos(\theta_1)$$

$$= g\cos(\theta_0)\cos(\omega_1 t+\varphi_1)+A_1\cos(\theta_1) +\frac{A_2}{2}\cos(\theta_0)\cos(\omega_2 t+\omega_1 t+\varphi_2+\varphi_1) +\frac{A_2}{2}\cos(\theta_0)\cos(\omega_2 t-\omega_1 t+\varphi_2-\varphi_1) \quad (2)$$

Wherein $\omega_2 = 2\pi f_2$, $f_2$ is the excitation and vibration frequency; $A_2 = \omega_2^2 H_2$, $H_2$ is the vibration amplitude at the position of the SD. The spectrum of any one component of the accelerometer output contains three components: $f_1, f_2+f_1$, and $f_2-f_1$.

Acceleration modulus square (AMS) of the three components, $|\mathbf{a}|^2$, is denoted as $a^2$. **Figure 3** shows the relationship of the acceleration modulus, $|\mathbf{a}|$, the vibration induced acceleration $A_2\cos(\omega_2 t+\varphi_2)$, the gravity acceleration $g$, and the centripetal acceleration $A_1$. $a^2$ can be expressed as:

$$\begin{aligned} a^2 &= [g+A_2\cos(\omega_2 t+\varphi_2)+A_1\cos(\omega_1 t+\varphi_1)]^2 \\ &\quad +A_1^2\sin^2(\omega_1 t+\varphi_1) \\ &= A_1^2+g^2+\frac{A_2^2}{2}+\frac{A_2^2}{2}\cos(2\omega_2 t+2\varphi_2) \\ &\quad +2gA_1\cos(\omega_1 t+\varphi_1)+2gA_2\cos(\omega_2 t+\varphi_2) \\ &\quad +A_1A_2\cos(\omega_2 t+\omega_1 t+\varphi_2+\varphi_1) \\ &\quad +A_1A_2\cos(\omega_2 t-\omega_1 t+\varphi_2-\varphi_1) \end{aligned} \quad (3)$$

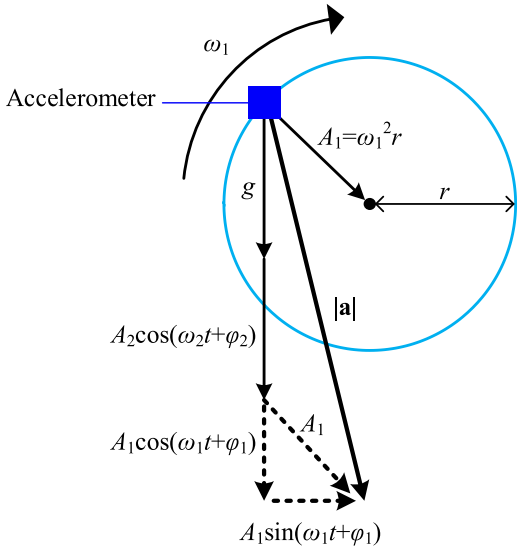


**FIGURE 3.** Acceleration synthesis in the rotation plane.

According to Eqs (2) and (3), the spectrums of the SAC $a_x$ and the AMS $a^2$ contain different characteristic frequency components. Their own amplitudes are listed in **Table 1**. $a^2$ has 5 characteristic frequencies, 4 of which contain the vibration frequency $f_2$. $a_1$ has 3 characteristic frequencies, 2 of which contain $f_2$. The amplitudes of $f_2+f_1$ and $f_2-f_1$ in $a^2$ are susceptible to the noise of $A_1$. The amplitudes of $f_2+f_1$ and $f_2-f_1$ in $a_x$ are susceptible to the noise of $\theta_0$. The amplitudes of $f_2$ and $2f_2$ in $a^2$ are only related to the vibration amplitude

**TABLE 1.** Characteristic frequencies of acceleration signals.

| Characteristic frequencies | Amplitude, in $a^2$ | Amplitude, in $a_x$ |
|---|---|---|
| $f_1$ | $2gA_1$ | $g\cos(\theta_0)$ |
| $f_2$ | $2gA_2$ | -- |
| $f_2+f_1$ | $A_1A_2$ | $\frac{A_2}{2}\cos(\theta_0)$ |
| $f_2-f_1$ | $A_1A_2$ | $\frac{A_2}{2}\cos(\theta_0)$ |
| $2f_2$ | $\frac{{A_2}^2}{2}$ | -- |

($g$ is constant) and is immune to $\theta_0$ and $A_1$, whose fluctuations represent the rotational noises, so their signal noise ratios (SNRs) are higher than other characteristic frequencies. With respect to $a^2$, the amplitude of $f_2$ is larger than those of $f_2+f_1$ and $f_2-f_1$, because the accelerometer has a small rotation radius and a low rotation speed, $A_1 = \omega_1^2 r \ll 2g$. For the SAC $a_x$, when the vibration amplitude $H_2$ is small, the amplitudes of $f_2+f_1$ and $f_2-f_1$ are much smaller than that of $f_1$, because $g \gg \frac{A_2}{2} = \frac{\omega_2^2 H_2}{2}$. Therefore, the frequency components $f_2+f_1$ and $f_2-f_1$ in $a_x$, which contain the vibration frequency $f_2$, can noticeably appear in the frequency spectrum only when the vibration is very severe.

$a^2$ contains more useful information than $a_x$ that can be used to detect the existence of the vibration frequency $f_2$. When $H_2$ is large enough, there will be five noticeable peaks in the frequency spectrum of $a^2$, and it is difficult to determine which peak is $f_2$ among the five. In the expression of $a^2$, the amplitudes of different frequencies that are related to $A_1$ are also related to $f_1$, and if the value of $A_1$ can be reduced, the amplitude of $f_1$ related can be suppressed and the amplitude of $f_2$ can be highlighted. There are two ways to reduce $A_1$: (1) Install the accelerometer at the center of the SD to have $r=0$, so $A_1 = \omega_1^2 r = 0$; (2) Remove $A_1$ via data post-processing.

The SD rolls with a constant angular speed in the pipeline for a certain period of time, during which the centripetal acceleration always points to the point B, as shown in **Figure** 2. As the angles between each of the three sensitive axes of the accelerometer and the rotation axis is unchanged, the projection of $A_1$ on each sensitive axis is the DC bias of each acceleration component. Removing the DC biases can eliminate $A_1$ and weaken the magnitudes of $f_1, f_2-f_1$ and $f_2+f_1$. The second method is more practical for field applications because the internal deployment of the SD has so many limitations in size, weight, and power supply that there

is no guarantee to install the accelerometer at the center of the ball. After removing the DC biases of the three acceleration components, $A_1 = 0$, the acceleration modulus square of AC components (AMS_AC), which are denoted as $\tilde{a}^2$, can be obtained:

$$\tilde{a}^2 = g^2 + \frac{A_2^2}{2} + \frac{A_2^2}{2}\cos\left(2\omega_2 t + 2\varphi_{2g}\right) + 2gA_2\cos\left(\omega_2 t + \varphi_{2g}\right) \quad (4)$$

## III. EXPERIMENTS

### A. SPECIFICATION SELECTION OF EXPERIMENTAL PIPE

The diameter of the subsea pipeline is usually larger than 200mm, and the spanning length is 10m ∼ 100m. The vortex induced vibration is the first-order mode and its frequency is very low, only a few hertz to several tens of hertz [9], [14]. For such a huge size, it is very difficult to build a subsea experiment system of ocean current impacts. Therefore, soft, small, short, and light PVC pipes are chosen to simulate the low-frequency first-order vibration of subsea spanning pipelines. Modal simulation analyses are carried out for steel pipes and PVC pipes with different specifications, in order to select suitable PVC pipe sizes so that the acceleration signals caused by the vibration of a small PVC pipe is identical to that of a subsea steel pipe.

The first-order resonance vibration frequency $f_n$ of the spanning pipeline with the spanning length of $l$ is [9]:

$$f_n = \frac{\pi}{2l^2}\sqrt{\frac{EI}{M_p + M_i + M_e}} \quad (5)$$

Wherein $E$ is the Young's modulus of elasticity, $I$ is the moment of inertia of an area, $M_i$ is the mass per unit length of the internal fluid along the pipeline, $M_p$ is the mass per unit length of the pipeline, and $M_e$ is the mass per unit length of the external additional fluid along the pipeline, and $M_e = \frac{C_m \pi \rho_e D^2}{4}$, where $C_m$ is the additional mass factor and $\rho_e$ is the external fluid density. The moment of inertia of the ring section is $I = \frac{\pi D^4(1-\alpha^4)}{64}$, where $\alpha = \frac{d}{D}$, $d$ and $D$ are the inner and outer diameters. $M_p = \rho_p\left(\pi D^2 - \pi d^2\right)/4$, $M_i = \rho_i \pi d^2/4$, where $\rho_i$ is the internal fluid density and $\rho_p$ is the pipe steel density.

Formula (5) can be further rewritten as:

$$f_n = \frac{\pi D}{8l^2}\sqrt{\frac{E(1-\alpha^4)}{\rho_p\left(1-\alpha^2\right) + \rho_i\alpha^2 + C_m\rho_e}} \quad (6)$$

It can be seen from Eq (6) that the resonance frequency $f_n$ of the spanning pipe is proportional to the outer diameter $D$ of the pipe, and is inversely proportional to the square of the spanning length $l$. Modal simulations were carried out for three common specification steel pipes: Φ219 mm × T6 mm, Φ330 mm × T8 mm, Φ474 mm × T12 mm. Their lengths were swept. Two ends of the steel pipes were configured as fixed constraints, and the first six vibration modes were calculated. According to the vibration shape, the resonance frequency of the first-order modal is determined. The resonance frequency as a function of the pipe length are shown in Figure 4(a). The resonance frequencies of the three steel pipes are 1Hz∼22Hz when the pipe lengths are 10m∼40m.

The PVC pipes to be used in the following experiments have three optional diameters: 50mm, 75mm, and 100mm. The Young's modulus of PVC is 3400MPa, and the density is 1380Kg/m$^3$. In the model simulations, two ends of the PVC pipes were configured as fixed constraints, and the first six vibration modes were calculated. The resonance frequency as a function of the PVC pipe length are shown in Figure 4(b). The resonance frequencies of the three PVC pipes are 1Hz∼22Hz when the pipe lengths are 1.5m∼7m. All of them can be used to simulate the vibration of the real subsea steel pipeline.

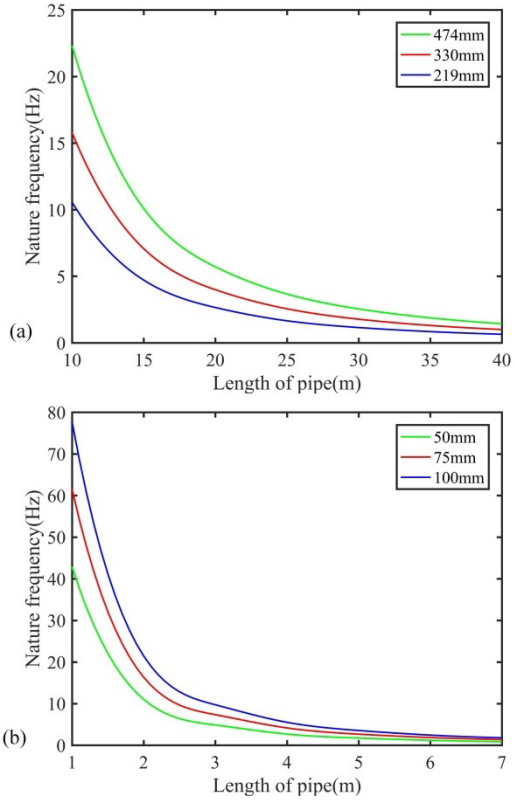


**FIGURE 4.** First-order modal frequencies vs lengths of pipes with different diameters: (a) steel pipes, (b) PVC pipes.

The PVC pipe with the diameter of 75mm is chosen, and the diameter of the mini SD accounts for 60%∼80% of the pipe diameter. The mini SD can get enough thrust from the flow and have enough space to deploy the accelerometer and batteries. Considering that the SD has to roll enough circles in the pipe in order to get adequate sampling length in time domain and the space limitation of the experimental site, the PVC pipe length is finally chosen to be 4 m.

### B. EXPERIMENT METHOD AND PROCESS

As shown in **Figure** 5, an electromagnetic exciter is used to excite the PVC pipe to vibrate like the vortex-induced

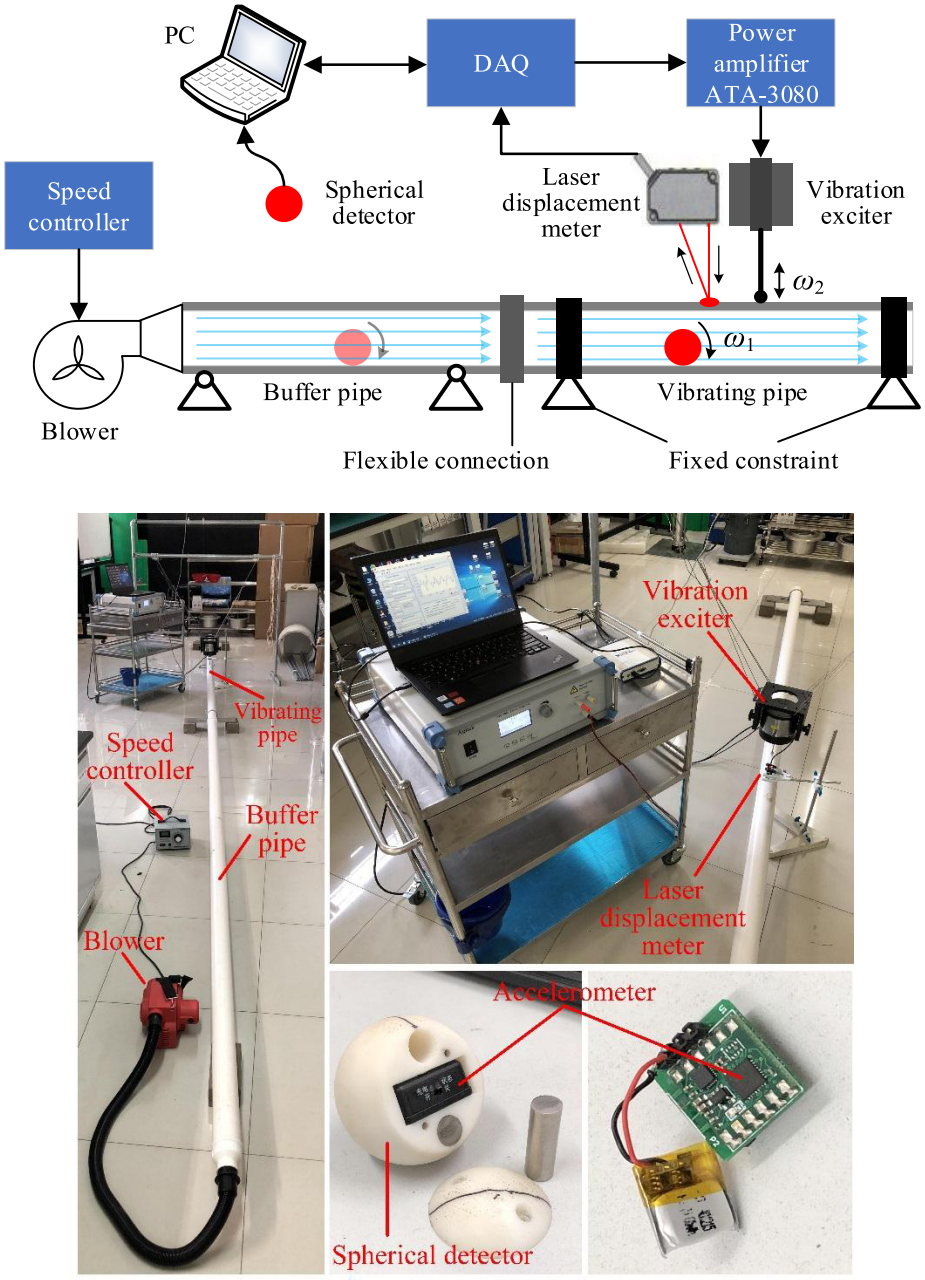


**FIGURE 5.** Schematic and photos of experiments.

vibration of the spanning subsea pipeline. The pipe sizes are chosen according to simulation results above to make the resonance frequency of the experimental pipe be close to that of the subsea spanning pipeline. A mini SD equipped with a triaxial accelerometer is used to sense the pipe vibrations. Two steel columns are inserted in the SD to adjust the mass distribution so that the SD can stably rotate around the axis of the largest inertia among the three. A laser displacement meter measures the vibration displacement of the pipe in real time as a reference. Considering that the SD has a speed-up process, a buffer pipe is connected to the upstream end of the tested pipe to help the SD reach the steady rolling state with a constant rolling speed before entering the tested pipe. The two ends of the tested pipe are fixed onto the floor to simulate the actual spanning subsea pipeline being bound by the soil.

## IV. RESULTS AND DISCUSSIONS

### A. ACCELERATION SIGNALS IN TIME DOMAIN

The SD's rotation axis is almost parallel to one of the three sensitive axes of the accelerometer, as the amplitude of the red component is much smaller than the blue and green ones, as shown in **Figure** 6(a). The three curves represent the three

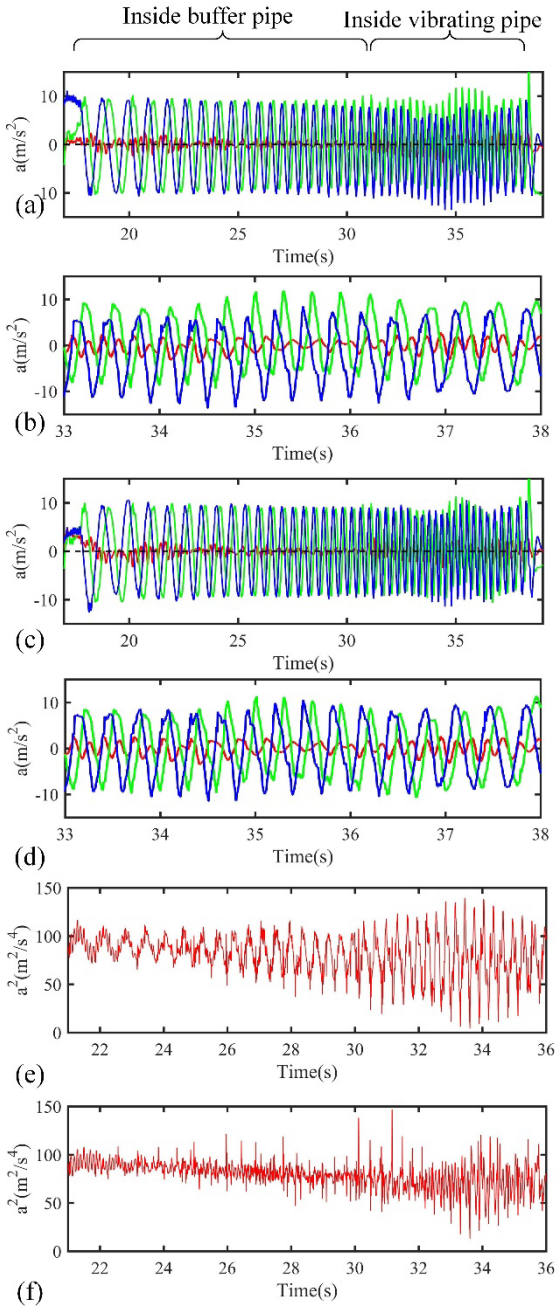


**FIGURE 6.** Acceleration signals of one test in time domain: (a) and (b) are raw three-component data, (e) is raw modulus data, and (c) (d) (f) are data with DC biases removed.

acceleration components measured by the accelerometer. The rotation speed of the SD becomes stable from about 30 s. The acceleration period of the first 2/3 samples is gradually reduced, and these samples are collected during the speed-up process in the buffer pipe. The acceleration period of the last 1/3 samples is very stable, and these samples are acquired when the SD rolls in the tested pipe.

A high frequency signal is superimposed on the low frequency signal, as shown in **Figure** 6(b), where the acceleration signals in the excited pipe are zoomed in with respect to the time axis. They stem from the pipe vibration and the SD rotation, respectively. The green and blue components have significant DC biases, which are the projections of the rotational centripetal acceleration of the accelerometer on these two sensitive axes. Wavelet decomposition and reconstruction method is used to remove the DC bias, and the results are shown in **Figure** 6(c) and (d). Before removing the DC bias, the local average of the acceleration signal is not zero, and the signal has noticeable fluctuations. After the DC bias is removed, the acceleration waveform at each moment is almost symmetric about the horizontal axis. At the same time, the additional high frequency details on the low frequency signal are perfectly preserved. Many wavelet bases can work well for removing the DC biases. This paper employ the ''db05'' base. The number of decomposition layers is 8. The coefficients of all layers except the layer corresponding to the lowest frequency are used by the reconstruction.

Removing the DC bias of the acceleration signals can significantly suppress the $f_1$ frequency component. As can be seen from **Figure** 6(e) and (f), before removing the DC bias of each component, the AMS $a^2$ contains a very strong low frequency component representing the SD rotation, and also contains some other high-frequency components. After removing the DC biases, $a^2$ becomes the AMS_AC $\tilde{a}^2$, which is equivalent to removing the centripetal acceleration, and the low frequency component related to $f_1$ almost disappears. $\tilde{a}^2$ contains significant high frequency information representing the pipeline vibration, which can be used to identify the vibration. This verifies the analysis results of Eqs (3) and (4).

### *B. COMPARISON OF THE ABILITIES OF $a_x$, $a^2$, $\tilde{a}^2$ TO DETECT $f_2$*

Different frequencies and amplitudes of excitations were applied to the pipe in order to compare the SNRs of $a_x$ and $a^2$ when using $f_2$ related components to indicate the pipe vibration. The SNRs of each experiment results and their frequency spectrums are shown in **Figure** 7. Among them, $f_1$ corresponds to the rotation frequency of the SD, and $f_2$ corresponds to the excitation and vibration frequency. As shown in **Figure** 7(a), $a^2$ can detect the pipeline vibration in all three cases, while $a_x$ can only detect the 10Hz and 15Hz vibrations, and the SNR of $a^2$ is greater than that of $a_1$. Here, the SNR is defined as the ratio of the amplitude of the $f_2$ related ($f_{2r}$) component to the noise floor that is the mean value of the frequency spectrum in the ranges of $[f_{2r} - 2\text{Hz}, f_{2r} - 0.5\text{Hz}]$ and $[f_{2r} + 0.5\text{Hz}, f_{2r} + 2\text{Hz}]$. $f_{2r}$ can be $f_2$ itself, or $2f_2, f_2 + f_1, f_2 - f_1$.

For the 5 Hz excitation, as shown in **Figure** 7(b) and (c), $a_x$ in the frequency domain does not show any information about $f_2$, so the SNR is 0. In contrast, $a^2$ in the frequency domain has two distinct peaks at $f_2$ and $2f_2$, and its SNR is calculated by using $f_2$. For the 10 Hz excitation, as shown in **Figure** 7(d) and (e), $a_x$ has two sharp peaks at $f_2 + f_1$ and $f_2 - f_1$, and the SNR is calculated by using $f_2 + f_1$. In contrast, $a^2$ has two sharper peaks at $f_2$ and $f_2 - f_1$, and one peak at $f_2 + f_1$, and

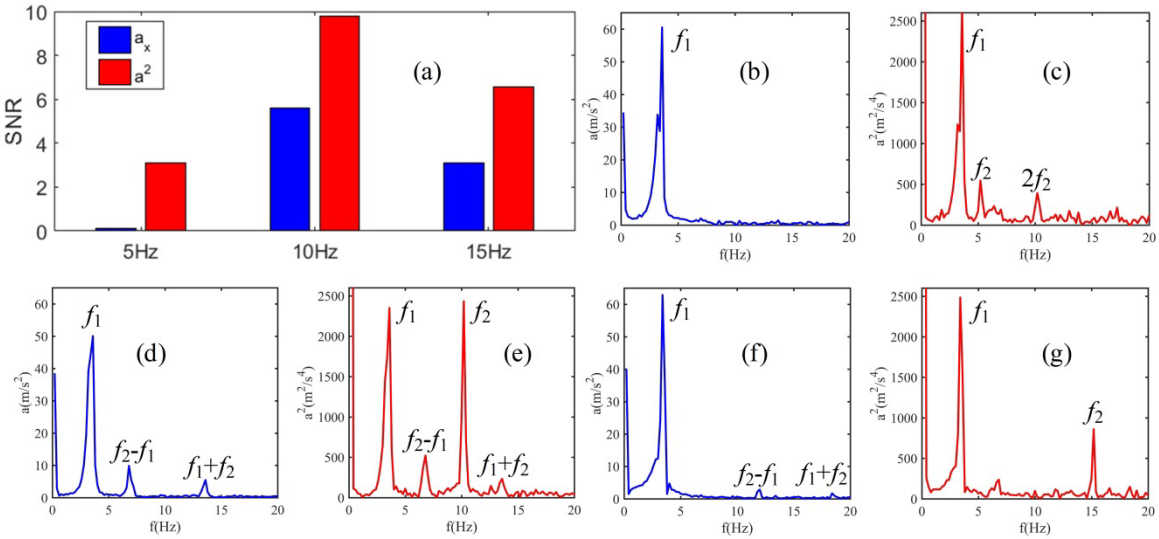


**FIGURE 7.** SNR comparisons of $a_x$ and $a^2$ under different excitation frequencies: (b) and (c), $f_2 = 5$Hz; (d) and (e), $f_2 = 5$Hz; (f) and (g), $f_2 = 5$Hz.

the SNR is calculated by using $f_2$. For the 15 Hz excitation, as shown in **Figure** 7(f) and (g), $a_x$ has two obscure peaks at $f_2+f_1$ and $f_2-f_1$, and the SNR is calculated by using $f_2+f_1$. In contrast, $a^2$ has a pretty noticeable peak at $f_2$, and the SNR is calculated by using $f_2$.

In all of these experiments, $f_2$ in $a^2$ always exists very clearly, while other frequency components containing $f_2$ in both $a_x$ and $a^2$ do not always appear, or even if they appear, their SNRs are lower than that of $f_2$. Once again this verifies the conclusion of the analyses of **Table 1** in Section 2: the amplitude of $f_2$ in $a^2$ is only related to the vibration amplitude, and will not be disturbed by the rotating noise of the SD. The SNR of $f_2$ in $a^2$ is higher.

If the vibration amplitude of the pipeline is larger, the vibration in the frequency spectrum is more noticeable, and it is more beneficial for spanning vibration detections. However, too large vibration amplitude may result in extra interferential peaks in the frequency spectrum. It is sophisticated to automatically judge by using the computer to identify which one among the five is the peak of $f_2$, when the excitation or vibration amplitude is very large and the frequency spectrum of $a^2$ contains five peaks. The peak of $f_1$ indicating the SD rolling can be easily identified by the acceleration signals collected inside other non-vibrating pipe segments, because these signals only contain the $f_1$ component. The other four peaks are at $f_2$, $2f_2$, $f_2+f_1$, and $f_2-f_1$. The amplitudes of the last three are susceptible to many factors, and may be either lower or higher than the amplitude of $f_2$. According to Eq. (4), by removing the DC bias of each acceleration component, $\tilde{a}^2$ is obtained, and the amplitudes of $f_1, f_2+f_1$, and $f_2-f_1$ is significantly weakened only with the $f_2$ and $2f_2$ peaks preserved. As shown in **Figure** 8, the red curve is the frequency spectrum of $\tilde{a}^2$ with the DC bias of each component removed, and the blue curve is the spectrum

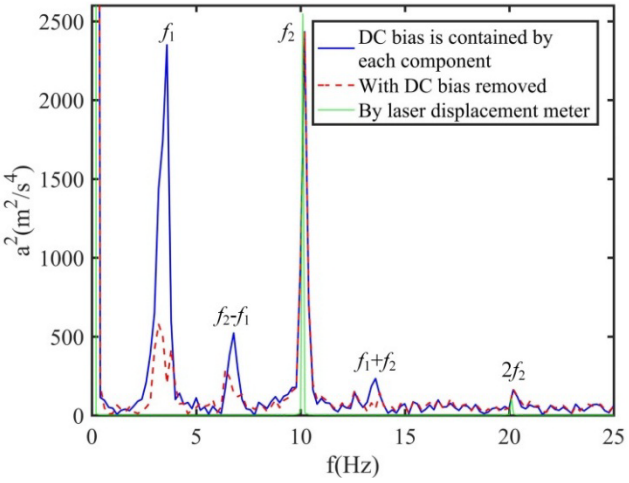


**FIGURE 8.** Role of removing the DC bias in each acceleration component.

of $a^2$ with the DC biases preserved. Noticeably, by removing DC biases, the peaks of $f_1, f_2+f_1$ and $f_2-f_1$ are significantly weakened, while the peaks of $f_2$ and $2f_2$ are unchanged. $f_2$ and $2f_2$ can be easily determined, and then $f_2$ can be further confirmed via the relationship of $2f_2/f_2 = 2$.

### C. ACCURACY AND RESOLUTION OF USING $\tilde{a}^2$ TO DETECT f2

Removing DC biases can contribute to determining the value of $f_2$ without resulting in principle errors. The accuracy of employing $f_2$ to detect the pipe vibration (frequency) was further studied and demonstrated. **Table** 2 shows the measurement results and relative errors when the excitation frequency is 5 Hz $\sim$ 15 Hz. It can be seen that there is a fixed bias error of about 0.16 Hz, which is equal to the frequency resolution

**TABLE 2. Measurement accuracy of pipe vibration frequency $f_2$.**

| Excitation Frequency(Hz) | Measured $f_2$(Hz) | Relative Error |
|---|---|---|
| 5 | 5.16 | 3.25% |
| 6 | 6.08 | 1.30% |
| 7 | 7.16 | 2.30% |
| 8 | 8.16 | 2.00% |
| 9 | 9.16 | 1.77% |
| 10 | 10.16 | 1.58% |
| 11 | 11.16 | 1.43% |
| 12 | 12.16 | 1.30% |
| 13 | 13.16 | 1.20% |
| 14 | 14.15 | 1.11% |
| 15 | 15.15 | 1.03% |

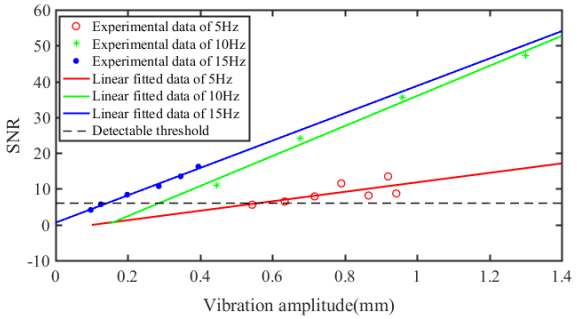


**FIGURE 9. Detectable vibration thresholds for different frequencies.**

$\delta f$ of the Fourier transform. $\delta f = f_s/N = 1/T$, where $f_s$ is the sampling frequency, $N$ is the number of sampling points, and $1/T$ is the length of sampling duration. $T = 5\text{s}\sim6\text{s}$ as shown in **Figure** 6(b) and (d). Therefore, the measurement accuracy of the vibration frequency $f_2$ is very high.

When the vibration is too weak, the vibration induced acceleration signals may be immerged in the noise and is difficult to identify. The SNR of $f_2$ in $\tilde{a}^2$ at different excitation intensities was investigated to determine the threshold of $\tilde{a}^2$ for detecting the pipe vibration. The excitation frequency was fixed at 5Hz, 10Hz, and 15Hz, respectively. For each frequency of excitation, the excitation voltage was linearly changed to obtain the SNR at different amplitudes. The results are shown in **Figure** 9. It can be seen that the SNR is proportional to the vibration amplitude of the pipe when the excitation frequency is fixed. A large number of experimental results show that for the peak of $f_2$, when the SNR is larger than 5, the peak of $f_2$ can be reliably identified and the value of $f_2$ can be correctly obtained. Taking SNR $= 5$ as the boundary, the detectable vibration amplitude thresholds are 0.6 mm, 0.4 mm, and 0.2 mm for 5 Hz, 10 Hz, and 15 Hz excitations, respectively, under the current experimental conditions. Larger noises will increase the detection thresholds.

## V. CONCLUSIONS

This paper proposes a method for detecting the vibration of subsea spanning pipelines by using a SD. Mathematical analyses and experiments demonstrate that: (1) $a_x$ contains two frequency components, $f_2 + f_1$ and $f_2 - f_1$, which can indirectly indicate pipeline vibrations; while besides of $f_2+f_1$ and $f_2 - f_1$, $a^2$ contains $f_2$ and $2f_2$ that can directly indicate pipeline vibrations; (2) Further, by removing the DC bias of each component to calculate $\tilde{a}^2$, the interference of the centripetal acceleration to the identification of $f_2$ can be eliminated; (3) The SNR of $f_2$ in $a^2$ and $\tilde{a}^2$ is higher than that of $f_2+f_1$ and $f_2-f_1$ in $a_x$, so $f_2$ can be accurately and sensitively identified by using the $\tilde{a}^2$; (4) The detection thresholds of 5 Hz, 10 Hz, and 15 Hz vibrations are 0.6 mm, 0.4 mm, and 0.2 mm with regard to the amplitude, respectively.

## REFERENCES

[1] P. Davis and J. Brockhurst, "Subsea pipeline infrastructure monitoring: A framework for technology review and selection," *Ocean Eng.*, vol. 104, pp. 540–548, Aug. 2015.
[2] A. Zakeri, "Review of state-of-the-art: Drag forces on submarine pipelines and piles caused by landslide or debris flow impact," *J. Offshore Mech. Arctic Eng.*, vol. 131, no. 1, pp. 403–410, 2009.
[3] J. Cai, X. Jiang, and G. Lodewijks, "Residual ultimate strength of offshore metallic pipelines with structural damage—A literature review," *Ships Offshore Struct.*, vol. 12, no. 8, pp. 1037–1055, 2017.
[4] Y. Wu and Y.-M. Chiew, "Mechanics of three-dimensional pipeline scour in unidirectional steady current," *J. Pipeline Syst. Eng. Pract.*, vol. 4, no. 1, pp. 3–10, Feb. 2013.
[5] L. Cheng, K. Yeow, Z. Zang, and F. Li, "3D scour below pipelines under waves and combined waves and currents," *Coastal Eng.*, vol. 83, pp. 137–149, Jan. 2014.
[6] T. Li, C. An, W. Liang, M. Duan, and S. F. Estefen, "Semi-analytical solution for soil-constrained vibration of subsea free-spanning pipelines," *Ships Offshore Struct.*, vol. 13, no. 6, pp. 666–676, Apr. 2018.
[7] M. Mandal and P. Roy, "Influence of pipeline specifications and support conditions on natural frequency of free spanning subsea pipelines," *Adv. Struct. Eng.*, vol. 1, pp. 663–672, Jan. 2015.
[8] K. Kamran, "Vortex induced vibrations of free span pipelines," Ph.D. dissertation, Dept. CeSOS, Norwegian Univ. Sci. Technol., Trondheim, Norway, 2009.
[9] C. Bowen, S. Li, and G. Fan, "Maximum allowable span length calculation for submarine pipelines," *J. Disaster Prevention Mitigation Eng.*, vol. 30, pp. 291–293, Sep. 2010.
[10] D.-Y. Zhao, L. Zhou, N. He, and F.-Y. Wang, "Hydrodynamic forces and instability of submarine pipelines under waves and currents: A review," *China Ocean Eng.*, vol. 24, no. 2, pp. 391–400, 2010.
[11] E. V. M. dos Reis, L. A. Sphaier, L. C. S. Nunes, and L. S. de B. Alves, "Dynamic response of free span pipelines via linear and nonlinear stability analyses," *Ocean Eng.*, vol. 163, pp. 533–543, Sep. 2018.
[12] M. M. Shabani, A. Taheri, and M. Daghigh, "Reliability assessment of free spanning subsea pipeline," *Thin-Walled Struct.*, vol. 120, pp. 116–123, Nov. 2017.
[13] M. Drago, M. Mattioli, R. Bruschi, and L. Vitali, "Insights on the design of free-spanning pipelines," *Philos. Trans. Roy. Soc. A, Math., Phys. Eng. Sci.*, vol. 373, no. 2033, p. 20140111, 2015.
[14] Z.-G. Xiao and X.-L. Zhao, "Prediction of natural frequency of free spanning subsea pipelines," *Int. J. Steel Struct.*, vol. 10, no. 1, pp. 81–89, 2010.
[15] J.-S. Hu, X. Feng, X. Li, and J. Zhou, "Condition identification based on vibration measurements for free spanning submarine pipelines," *China Ocean Eng.*, vol. 22, no. 4, pp. 561–574, Dec. 2008.

[16] J. Y. Lee, J. McInerney, R. Cossu, Z. Q. Leong, and A. L. Forrest, "Predicting scour beneath subsea pipelines from existing small free span depths under steady currents," *J. Ocean Eng. Sci.*, vol. 2, no. 2, pp. 61–75, Jun. 2017.
[17] N. F. Braathen and A. J. Sandford, "Pipeline inspection by ROV," in *Submersible Technology* (Advances in Underwater Technology, Ocean Science and Offshore Engineering), vol. 5. Dordrecht, The Netherlands, Springer, 1986, pp. 313–318.
[18] Z. Wenjing, X. Yuru, W. Lei, and Z. Tiedong, "Optical vision pipeline inspection and tracking system for autonomous underwater vehicle," *J. Shanghai Jiao Tong Univ.*, vol. 46, no. 2, pp. 178–183, 2012.
[19] X. Huang, Y. Li, and S. Jin, "A control system based on data exchange using ethernet and CANBUS for deep water AUV," in *Proc. 9th Asian Control Conf. (ASCC)*, Jun. 2013, pp. 1–5.
[20] J. Quarini and S. Shire, "A review of fluid-driven pipeline pigs and their applications," *Proc. Inst. Mech. Eng. E, J. Process Mech. Eng.*, vol. 221, no. 1, pp. 1–10, 2007.
[21] H. S. Han, J. J. Yu, C. G. Park, and J. G. Lee, "Development of inspection gauge system for gas pipeline," *KSME Int. J.*, vol. 18, no. 3, pp. 370–378, 2004.
[22] B. Han, D. Tan, Z. Jiang, L. Li, and X. Zhu, "Monitoring of vortex-induced vibration based on fiber Bragg grating technology for pipelines subjected to flood impacting," in *Proc. 32nd Chin. Control Conf. (CCC)*, Jul. 2013, pp. 7357–7360..
[23] X. Nie, Y. Yang, Y. Cui, and C. Chen, "Long-term monitoring system of submarine pipeline vibration based on fiber grating sensor technology," in *Proc. Int. Offshore Polar Eng. Conf.*, Jun. 2018, pp. 230–237.
[24] L. Ren, Z. Jia, M. S. C. Ho, T. Yi, and H. Li, "Application of fiber Bragg grating based strain sensor in pipeline vortex-induced vibration measurement," *Sci. China Technol. Sci.*, vol. 57, no. 9, pp. 1714–1720, Sep. 2014.
[25] D. Maraval, R. Gabet, Y. Jaouen, and V. Lamour, "Dynamic optical fiber sensing with Brillouin optical time domain reflectometry: Application to pipeline vibration monitoring," *J. Lightw. Technol.*, vol. 35, no. 16, pp. 3296–3302, Aug. 15, 2017.
[26] P. Rajeev, J. Kodikara, W. K. Chiu, and T. Kuen, "Distributed optical fibre sensors and their applications in pipeline monitoring," *Key Eng. Mater.*, vol. 558, pp. 424–434, Jun. 2013.
[27] P. Job and M. Hawkins, "*In-situ* vibration monitoring of pipeline freespans," in *Proc. Int. Conf. Offshore Mech. Arctic Eng.*, vol. 3, 2008, pp. 351–360.
[28] L. Baojun, S. Xiaohong, W. Haiyan, and J. Zhe, "One novel monitoring method for free span of subsea pipeline," in *Proc. OCEANS-TAIPEI*, Apr. 2014, pp. 1–6.
[29] L. Baojun, S. Xiaohong, W. Haiyan, and J. Zhe, "One parallel UAN architecture for monitoring free span of deep-water subsea pipelines," in *Proc. OCEANS-TAIPEI*, Apr. 2014, pp. 1–5.
[30] N. Liao, Q. Ding, H. Zhang, S. Du, S. Zhang, and B. Tang, "A method for identifying free span of subsea pipelines," in *Proc. Int. Offshore Polar Eng. Conf.*, 2017, pp. 193–199.
[31] F. Richard and C. Muthu, "SmartBall: A new approach in pipeline leak detection," in *Proc. Biennial Int. Pipeline Conf. (IPC)*, vol. 2, 2009, pp. 117–133.
[32] S. X. Guo, S. L. Chen, X. J. Huang, and T. S. Xu, "Design of a spherical leak detector for submarine oil pipelines," *Appl. Mech. Mater.*, vol. 709, pp. 460–464, Dec. 2015.
[33] S. Guo, S. Chen, X. Huang, Y. Zhang, and S. Jin, "CFD and experimental investigations of drag force on spherical leak detector in pipe flows at high Reynolds number," *Comput. Model. Eng. Sci.*, vol. 101, no. 1, pp. 59–80, 2014.
[34] X. Huang *et al.*, "A 3D localization approach for subsea pipelines using a spherical detector," *IEEE Sensors J.*, vol. 17, no. 6, pp. 1828–1836, Mar. 2017.
[35] Z. Yu, X. Yameng, H. Xinjing, L. Jian, and C. Shili, "Pipeline inclination measurements based on a spherical detector with magnetic proximity switches," *IEEE Access*, vol. 6, pp. 39936–39943, 2018.
[36] X. Huang, G. Chen, Y. Zhang, J. Li, T. Xu, and S. Chen, "Inversion of magnetic fields inside pipelines: Modeling, validations, and applications," *Struct. Health Monitor.*, vol. 17, no. 1, pp. 80–90, 2017.

**GUO LIN** received the B.E. degree from the Harbin Institute of Technology, in 2010, and the M.E. degree from Sun Yat-sen University, in 2014. He is currently pursuing the Ph.D. degree with Tianjin University. His research subject is the span inspection of subsea pipelines.

**ZENG ZHOUMO** received the Ph.D. degree from Tianjin University (TJU), in 1993. He is currently a Professor with TJU, where he is also the Dean of the School of Precision Instrument and Opto-Electronics Engineering. His research subjects are detection technology and instrument, system integration and intellectualization, and MEMS.

**HUANG XINJING** received the B.S. and Ph.D. degrees from Tianjin University (TJU), in 2010 and 2016, respectively. He is currently an Assistant Professor with TJU. His research interest includes pipeline damage detections.

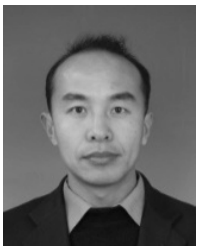

**LI JIAN** received the B.E., M.E., and Ph.D. degrees from Tianjin University (TJU), in 1994, 1997, and 2000, respectively. He is currently a Professor with TJU. His research interests include pipeline leak detection and pipeline safety warning.

**CHEN SHILI** received the B.S. and Ph.D. degrees from Tianjin University (TJU) in 1997 and 2003, respectively. He is currently an Associate Professor with TJU. His research interest includes novel online in-pipe detector.